The Transantarctic Mountains Northern Network (TAMNNET): Deployment and Performance of a Seismic Array in Antarctica

by Samantha E. Hansen, Angela M. Reusch, Timothy Parker, Douglas K. Bloomquist, Paul Carpenter, Jordan H. Graw, and Gregory R. Brenn

INTRODUCTION

Over the past ~17 years, significant technological developments have advanced seismic investigations of the polar regions. In Antarctica, studies using data from a number of large-scale deployments, such as the Transantarctic Mountains Seismic Experiment (TAMSEIS), the Gamburtsev Antarctic Mountains Seismic Experiment (GAMSEIS), and the Polar Earth Observing Network (POLENET), have greatly improved our knowledge of the continent's tectonic evolution (Fig. 1). However, these studies have also illustrated that there is still a great deal more to be learned.

One of the goals of TAMSEIS was to investigate the origin of the Transantarctic Mountains (TAMs), the transcontinental mountain range that separates East and West Antarctica (Fig. 1; Robinson and Splettstoesser, 1986). The TAMs lack any evidence for a compressional origin, making their uplift history a matter of considerable debate; and, although many mechanisms have been proposed, there is little consensus on the TAMs tectonic history. Studies using TAMSEIS data investigated these questions, but the seismic array only crossed a small portion of the TAMs, leading to uncertainties about the crustal and upper-mantle structure beneath the remainder of the mountain range (Lawrence *et al.*, 2006a,b; Watson *et al.*, 2006; Reusch *et al.*, 2008; Hansen *et al.*, 2009; Pyle *et al.*, 2010). The more recent POLENET deployment has improved coverage of the southerly portion of the TAMs, but this network does not provide any coverage of the northern segment of the TAMs. The northern TAMs are an important section of the mountain range because they border the Ross Sea embayment, a major component of the West Antarctic rift system (Fig. 1).

In November–December 2012, the new Transantarctic Mountains Northern Network (TAMNNET; Fig. 1) was deployed to fill a gap in the seismic coverage in the northern TAMs, offering the capability to study this previously unexplored portion of the mountain range. Two years of continuous data have been acquired from this 15-station seismic array, which extends from Terra Nova Bay, inland across the TAMs, and into East Antarctica; an additional year of data will be collected in late 2015. Here, we report on the deployment, operation, and performance of TAMNNET, highlighting the technical aspects of the array, example seismic records, and data quality measurements.

EXPLORATION AND GEOLOGIC BACKGROUND

History of Antarctic Seismic Deployments

Both the Worldwide Standardized Seismograph Network and the later Global Seismographic Network (GSN) have provided global seismic coverage since the mid-1960s (Butler *et al.*, 2004). However, Antarctica has presented a large hole in the distribution of seismic stations, even up to the mid- to late-1990s, when only eight permanent GSN-style stations were deployed, primarily around the periphery of the continent. The first temporary broadband deployment in Antarctica was the Antarctic Network of Unattended Broadband Seismometers (ANUBIS) project, which installed six stations across West Antarctica between 1998 and 2001 (Fig. 1; Anandakrishnan *et al.*, 2000). New advancements were made in both power systems and data recording instrumentation to operate in the harsh polar climate. Specifically, photovoltaic panels and wind generators were used to recharge sealed lead-acid batteries to power the stations, and a custom data logging device with two hard disks provided long-term data storage because these stations could only be serviced about once per year. Güralp CMG-3ESP seismometers were buried within insulated boxes with timber frames to reduce temperature and environmental noise (Anandakrishnan *et al.*, 2000). However, despite these advancements, the ANUBIS stations only had a 50% uptime during the first year of deployment.

Building on the ANUBIS developments, the larger-scale (46 station; Fig. 1) TAMSEIS array was deployed between 2000 and 2003. All stations were equipped with broadband seismometers, typically Güralp CMG-3T instruments, as well as 24-bit REF TEK 72A-08 dataloggers (Pyle *et al.*, 2010). These stations were powered by both battery and solar systems during the austral summer months, but they did not record during the Antarctic winter (April–September) due to reduced power capabilities at colder temperatures. Heating elements were incorporated to stabilize the seismic equipment in the cold climate; however, given the difficulty of running instru-

doi: 10.1785/0220150117

mentation in such extreme conditions, many stations experienced downtime, so data availability is quite variable from station to station (Lawrence *et al.*, 2006a; Pyle *et al.*, 2010).

The advancement to year-round data recording in Antarctica came with technological developments for the GAMSEIS array (Fig. 1), a 30-station network deployed in 2007 in the extremely harsh environment high on the East Antarctic plateau. Both cold-rated Güralp CMG-3T and Nanometrics T-240 broadband sensors, along with Quanterra Q330 digital acquisition systems (DASs) with solid-state memory, were deployed (Heeszel *et al.*, 2013). A new station design (Johns *et al.*, 2006) was also incorporated, in which the seismometers were situated on insulated piers buried ~1 m below the snow surface, and insulated boxes were used to house the electronics and batteries. Similar to earlier deployments, solar panels (and in some cases, wind generators) were used to augment power and to recharge the lead-acid batteries during the austral summer, but primary power during the Antarctic winter was automatically switched to nonrechargeable lithium battery packs. A heat pad also supplied some additional heating, ultimately allowing the stations to maintain temperatures inside the insulated box that were 20°C or greater than the ambient temperature. These technological developments not only allowed for year-round data recording in Antarctica, but also led to an impressive ~93% data recovery (Heeszel *et al.*, 2013).

Similar to GAMSEIS, year-round data recording provided by the POLENET stations (Fig. 1) have greatly improved Antarctic seismic coverage. The first POLENET stations were also deployed in 2007, and many are still operating. Although most of these stations were installed in GAMSEIS-style snow vaults, some were installed on isolated rock outcrops throughout West Antarctica and within the TAMs (Anthony *et al.*, 2015). Given

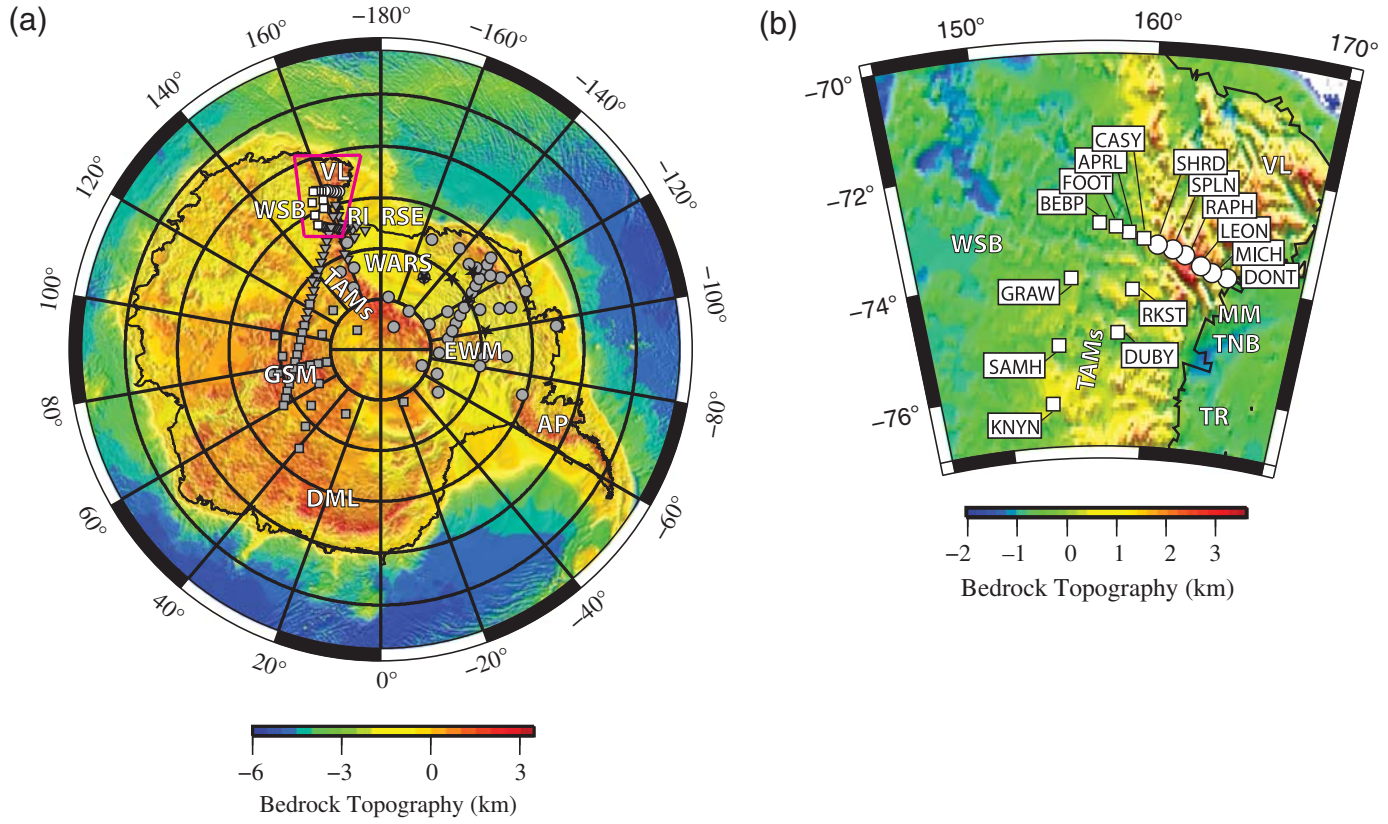

▲ **Figure 1.** (a) Subglacial bedrock topography from the BEDMAP2 model (Fretwell *et al.*, 2013). Shapes indicate stations from various seismic deployments across the continent (black stars, Antarctic Network of Unattended Broadband Seismometers [ANUBIS]; gray triangles, Transantarctic Mountains Seismic Experiment [TAMSEIS]; gray squares, Gamburtsev Antarctic Mountains Seismic Experiment [GAMSEIS]; gray circles, Polar Earth Observing Network [POLENET]; white circles and squares, Transantarctic Mountains Northern Network [TAMNNET]). The polygon highlights the region shown in (b). Key geographic features are labeled: TAMs, Transantarctic Mountains; WSB, Wilkes subglacial basin; VL, Victoria Land; RI, Ross Island; RSE, Ross Sea embayment; WARS, West Antarctic rift system; GSM, Gamburtsev Subglacial Mountains; DML, Dronning Maud Land; AP, Antarctic Peninsula; and EWM, Ellsworth–Whitmore Mountains. (b) Regional map focused on the TAMNNET deployment, with station names indicated. Additional geographic features not labeled in (a) include TR, Terror Rift; TNB, Terra Nova Bay; and MM, Mt. Melbourne. Stations denoted by circles are those powered with absorbed glass mat (AGM) batteries and two lampshade-style solar panel systems, whereas stations denoted by squares have one lampshade-style solar panel, one AGM battery, and 15 lithium battery packs. See text for further details.

the somewhat warmer environment in West Antarctica, the lower power (< 1.5 W) POLENET stations are only operated by lead-acid batteries and solar panel systems. Recent improvements have also allowed for greater data storage (16–128 GB) and iridium telemetry to monitor station performance (Parker *et al.*, 2008). All of these advancements have lead to the successful deployment of other temporary broadband arrays, such as TAMNNET, which is the focus of this article. Coupled with data from several of the aforementioned projects, data from TAMNNET allow for expanded investigations of the seismic structure beneath the central and northern TAMs.

Tectonic Setting: The Transantarctic Mountains

Reaching a height of ~4500 m, the TAMs extend approximately 4000 km across Antarctica (Fig. 1; Robinson and Splettstoesser, 1986). Apatite fission track dating indicates that the main phase of TAMs uplift began about 55 Ma, leading to as much as 7–8 km of uplift in some locations (Fitzgerald, 1992, 1994; Sutherland *et al.*, 2011), though the rate of uplift is still somewhat controversial (e.g., Barrett *et al.*, 1989; Clapperton and Sugden, 1990; Behrendt and Cooper, 1991). Additional constraints on the TAMs uplift history come from the Kukri peneplain. Near the mountain front, the peneplain had to be at a depth of ~3 km at the end of the Triassic to accommodate fluvial and shallow marine sediment deposition (Barrett, 1981); however, it is now found at elevations of 500–4000 m above sea level, indicating the extent of rock uplift. The lack of compressional structures in the TAMs has lead to considerable debate regarding their origin, and a variety of uplift mechanisms have been proposed (e.g., Fitzgerald *et al.*, 1986; ten Brink *et al.*, 1997; Studinger *et al.*, 2004; Karner *et al.*, 2005; Lawrence *et al.*, 2006b; Bialas *et al.*, 2007; Huerta and Harry, 2007; van Wijk *et al.*, 2008; Bialas, 2009).

The seismic velocity structure and the crustal thickness beneath the TAMs are key components to distinguish between competing uplift models. Regional-scale tomography results from TAMSEIS reveal a low-velocity, high-attenuation upper mantle concentrated beneath the Ross Island region but extending 50–100 km beneath the TAMs (Lawrence *et al.*, 2006a; Watson *et al.*, 2006). However, these models lose resolution away from Ross Island due to the limited aperture of the TAMSEIS deployment, making the lateral and depth extent of the upper-mantle anomaly difficult to constrain. Crustal thickness beneath the TAMs has been primarily investigated using *P*- and *S*-wave receiver functions (e.g., Bannister *et al.*, 2003; Lawrence *et al.*, 2006b; Hansen *et al.*, 2009). Beneath the central TAMs, the crust appears to thicken from 18–20 km beneath the Ross Sea coastline, immediately adjacent to the mountain range, to 40–45 km some 100–150 km inland. Beneath the more southerly TAMs, constraints from receiver functions and ambient noise tomography computed with POLENET data indicate Moho depths up to ~45 km beneath the TAMs, with thinner crust underlying the adjacent West Antarctic rift system (Fig. 1; Chaput *et al.*, 2014). None of these studies provide coverage of the northern TAMs, and additional characterization of the crustal and upper-mantle structure along this portion of the mountain front is necessary to more accurately assess competing origin models. The expanded seismic coverage provided by TAMNNET allows for such additional investigation.

TAMNNET DEPLOYMENT AND INSTRUMENTATION

As stated above, the 15 stations composing TAMNNET were initially deployed during the November–December 2012 Antarctic field season. The station locations were selected to maximize coverage of the study area and to optimize data recording while also maintaining operational feasibility. Ten stations, with ~30 km spacing, were deployed in a linear transect, starting near the coast ~50 km north of Mt. Melbourne and extending perpendicularly across the northern TAMs (Fig. 1). The orientation of this transect aligns with major sources of teleseisms around the Pacific. The remaining five stations were evenly distributed inland behind the TAMs front, further to the south, with one station (KNYN) reoccupying the former location of a previously deployed TAMSEIS station (E030). Three TAMNNET stations (DUBY, GRAW, and KNYN) were instrumented with Güralp cold-rated CMG-3T broadband seismometers, and Nanometrics Trillium 240 (T240) broadband instruments were installed at the remaining stations. Seismometers were enclosed within an insulated dome (Fig. 2). Each site was also equipped with a Quanterra Q330 DAS and a Packet Baler 44 storage drive, which are housed in an insulated enclosure. All stations include 12 different waveform channels, recording three-component data at four different sampling rates: 100, 40, 1, and 0.1 samples per second.

Stations operating at colder elevations on the East Antarctic plateau (Fig. 1) are powered by one SunXtender PVX-340T (34 Ah) absorbed glass mat (AGM) battery and 15 Tadiran lithium-thionyl chloride battery packs (190 Ah) during the dark winter months in Antarctica. During the summer months, power at each of these stations is also provided by a "lampshade-style" solar system (Fig. 2), which is outfitted with three Suntech monocrystalline silicon panels, capable of producing almost 40 W of solar power. Stations at warmer altitudes (Fig. 1) are powered by eight SunXtender PVX-1080T (108 Ah) and two PVX-340T AGM batteries, along with two lampshade-style solar panel systems. Figure 3 shows the variation of the DAS voltage and current with temperature for select stations. During the colder winter months, the AGM batteries cannot support the current flow at the same voltage, so the voltage drops when the current increases to maintain the system power requirements, as is shown for station SPLN in Figure 3a. However, for the stations deployed on the East Antarctic plateau (such as station GRAW, Fig. 3b), power is supplied by the primary lithium battery packs during the cold winter months, leading to an increase in voltage and a decrease in current.

The first year of continuous data was retrieved in November–December 2013. During servicing, Xeos iridium modems were added to each TAMNNET station, which provide real-time state-of-health (SOH) reports. These provide feedback on the Global Positioning System clock quality and phase error,

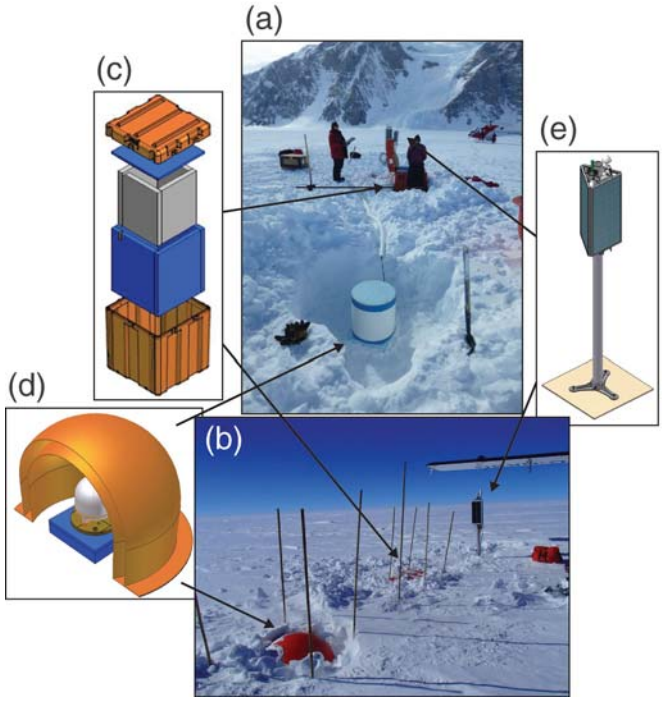

▲ **Figure 2.** (a) The installation of station DONT and (b) the final configuration of station FOOT. (c) Insulated enclosure that holds the electronics and batteries, (d) the insulated dome that covers the seismometer, and (e) the lampshade-style solar panel. Photos provided by (a) Douglas Bloomquist (Incorporated Research Institutions for Seismology–Program for the Array Seismic Studies of the Continental Lithosphere [IRIS-PASSCAL]) and (b) Samantha Hansen (The University of Alabama). Engineering diagrams provided by IRIS-PASSCAL (https://www.passcal.nmt.edu/content/polar/design-drawings, last accessed August 2015).

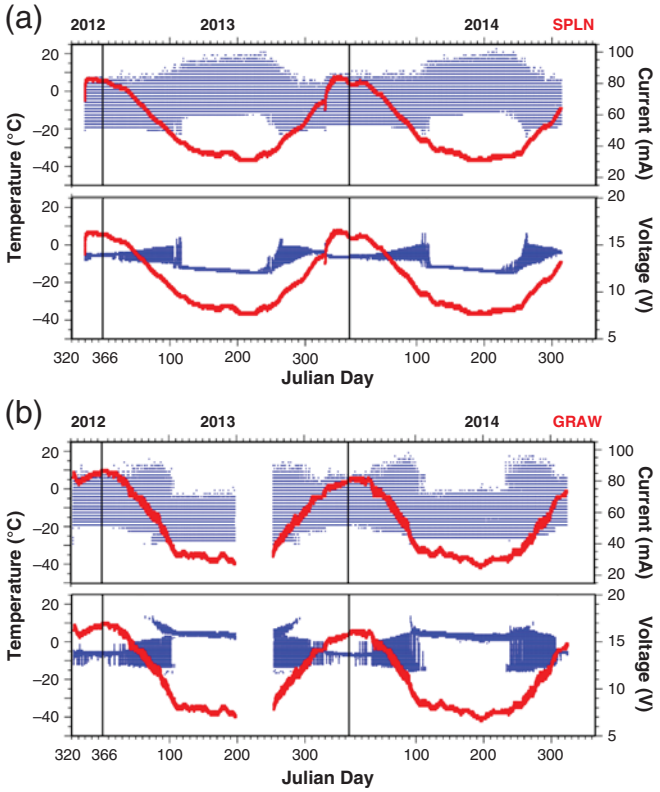

▲ **Figure 3.** Temperature (red) versus digital acquisition system (DAS) current and voltage (blue) for stations (a) SPLN and (b) GRAW as a function of deployment time. During the cold winter months (Julian day ~120–270), station SPLN displays a voltage drop and a current increase as the AGM batteries maintain the system power requirements. Station GRAW instead displays a voltage increase and current decrease during the winter months, when power is supplied by the primary lithium batteries. Station GRAW also shows a data gap during 2013, associated with the Q330 configuration issue, where the station turned off at temperatures below −40°C (see text for details).

current and voltage measurements, internal temperature, data transfer status, and the mass positions. Unfortunately, the seismometer at station KNYN malfunctioned and therefore was replaced with a T240 instrument. Also, a Q330 programming issue resulted in some stations (APRL, BEBP, CASY, FOOT, and GRAW) going off-line during the coldest winter months, when the temperature dropped below −40°C; however, these stations came back online once the weather warmed (Fig. 3), and the programming issue was corrected during the service season. Despite these issues, data recovery from the first year of operation was 91.2%. During November–December 2014, additional TAMNNET servicing occurred, and the second year of continuous data was acquired. Because the lithium-thionyl chloride batteries are not rechargeable, new packs were swapped into the associated stations to provide power for another year. Anomalously high, long-period (~50 s) noise was observed at station SHRD, which was originally installed with a T240 seismometer. It has been shown that the T240 instruments can experience unique seasonality issues in which long-period convection cells form on the vertical components during colder months, leading to additional noise (Anthony *et al.*, 2011, 2015); therefore, the sensor at this station was changed to a Güralp CMG-3T. Stations CASY and RAPH had some internal electrical issues (described in the next section), so most of the enclosure components were exchanged at these two stations to prevent future problems. Overall data recovery from the second year of deployment was 99.2%. The TAMNNET stations will continue to operate until late 2015, when they will be demobilized and removed from the field.

SEISMIC DATA QUALITY AND NOISE LEVELS

Both the SOH and the waveform files are monitored to assess TAMNNET data quality. Although highly decimated SOH files are available in real time, as mentioned above, waveform data can only be accessed in the field. During servicing, the 1 sample/s data at each site was visually inspected to assess any potential instrumentation problems. Most recorded data have excellent quality, with a high signal-to-noise ratio, like the examples shown in Figure 4. The SQLX spectral analysis

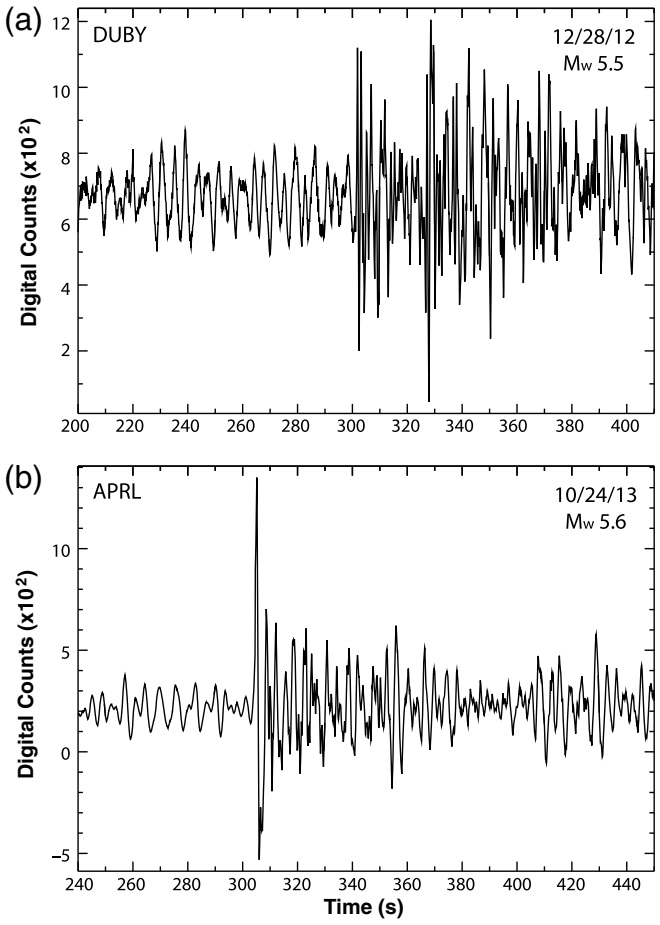

▲ **Figure 4.** Example TAMNNET waveforms. (a) Vertical component of station DUBY, showing an 5.5 earthquake that occurred on 28 December 2012 on the Minahassa Peninsula, Sulawesi (signal-to-noise ratio ≈ 3). (b) Vertical component of station APRL, showing an 5.6 earthquake that occurred on 24 October 2013 in the Kermadec Islands, New Zealand (signal-to-noise ratio ≈ 8).

tool (McNamara and Buland, 2004; Nanometrics, 2015) is also used to examine the noise power spectral density (PSD) at each station. This approach generates a probability density function (PDF) of the PSD distribution to estimate the background seismic noise. Signals from other sources, such as earthquakes, have lower probabilities and are mapped into the background level. Power values with high probabilities at each period reflect the ambient noise level and hence provide a measure of station quality (McNamara and Buland, 2004; Nanometrics, 2015). The PSD PDFs are referenced to the global high-noise model (HNM) and low-noise model (LNM) from Peterson (1993) for broader comparison. Three TAMNNET stations that experienced some operational issues (CASY, KNYN, and RAPH) are highlighted in Figures 5–7.

Both stations CASY and KNYN experienced problems with their installed seismometers. As stated previously, station CASY was outfitted with a Nanometrics T240 broadband sensor. The Trillium instruments include a symmetric triaxial force-feedback design in which two of the masses (VMV and VMW) contribute to all three sensor components, but the third mass (VMU) only affects the east and vertical components (Nanometrics, 2005). As shown in Figure 5, the SQLX spectral analysis plots for the east–west and vertical components are essentially flat across all periods, so it was suspected that there were problems with the VMU mass. However, examination of the SOH mass position records did not show any obvious issues with this channel compared with the other two masses (Fig. 5b). To avoid further problems, a new T240 seismometer was installed at station CASY during the 2014 service season. The original instrument was returned to Nanometrics for repair; it was later discovered that the pins inside the connector were pinched and therefore did not transmit the digital signals properly, ultimately affecting the VMU mass contribution to the seismic signal.

Station KNYN was outfitted with a Güralp CMG-3T instrument during the 2012 installation. When serviced the following year, a large bimodal noise response was observed on the vertical component, particularly at periods greater than ~10 s. Closer examination of the vertical component showed random, large-amplitude ~120 s pings that, in some cases, occurred hundreds of times per day (Fig. 6). For this reason, the seismometer at station KNYN was replaced with a T240 instrument, which improved the vertical-component noise condition. It should be noted that noise on the horizontal components is somewhat increased at the longest periods with the new sensor (Fig. 6), but this station has been performing well since the 2013 service season.

Station RAPH experienced a different type of problem. Although this station performed well during the 2012–2013 deployment season, the waveform data from the 2013–2014 season are riddled with gaps and spikes, denoting system reboots (Fig. 7b). At first, we suspected that there was a problem with the seismometer at this site, but examination of the mass positions (Fig. 7a) showed that they were very stable, with few (if any) recenters. Also, we compared waveform data from two 6.0 earthquakes, one from each field season, and found that the records have similar signal quality (Fig. 7c,d), despite the issues seen on the longer-duration waveform data during 2013–2014. The corresponding SQLX analysis (Fig. 7e,f) also illustrates that the noise condition at station RAPH is relatively stable. Therefore, the seismometer was ruled out as the problematic component.

When station RAPH was installed in 2012, the equipment was transported via an A-star helicopter, with the enclosure carried in a sling load. Given the high elevation of this station (~3100 m), the helicopter had difficulty maintaining altitude, and the enclosure was dropped, causing some of the internal vacuum panels to break. Therefore, when the site was serviced in 2013, it was decided that a new enclosure should be swapped in for the original one. Unfortunately, this new enclosure had a bad connector, leading to an electrical issue that caused the DAS to reboot frequently, which is seen by the various gaps and spikes in the data (Fig. 7b). The timing of when these problems started to occur is coincident with the 2013 servicing. By combining the waveform data and the SOH files, our team was able to accu-

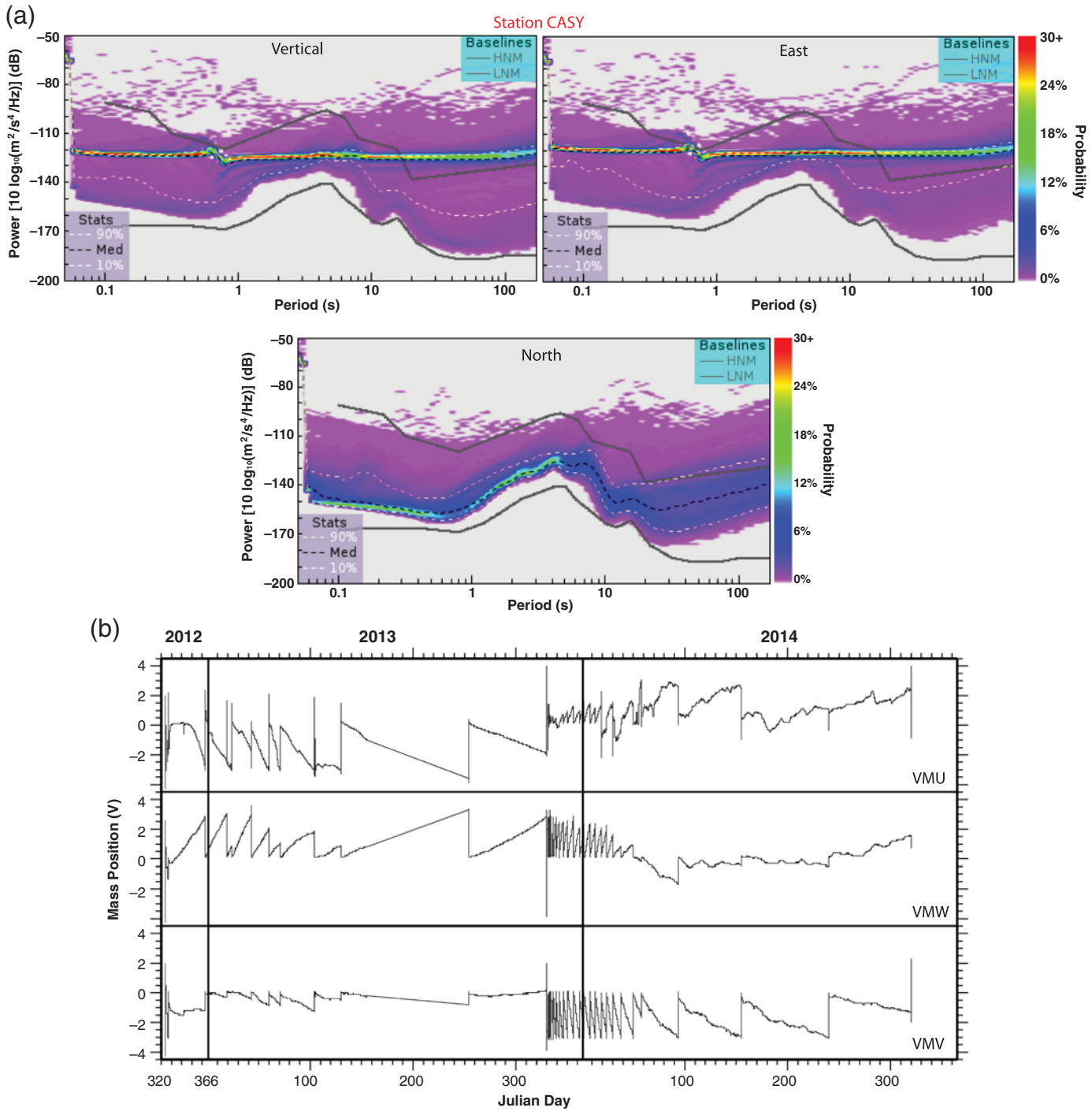

▲ **Figure 5.** (a) SQLX spectral analysis results for each component of station CASY. On each panel, the black and white dashed lines mark the median and the 90th/10th percentiles of the computed probability density functions (PDFs), respectively. The gray lines denote the high-noise model (HNM) and low-noise model (LNM) baselines (Peterson, 1993; McNamara and Buland, 2004; Nanometrics, 2015). The power spectral density (PSD) PDFs correspond to the time period between 19 November 2012 and 16 November 2014. (b) Corresponding plots of mass positions versus deployment time. Despite the issues seen on the east–west and vertical PSD PDFs in (a), all three mass position signals are comparable.

rately diagnose the problem and to fix the necessary components during the 2014 service season. Overall, having the capability to assess these records while in the field allowed for rapid identification and correction of equipment issues.

SUMMARY

Building on ~17 years of technological advancements, the capabilities of polar seismology have been greatly improved.

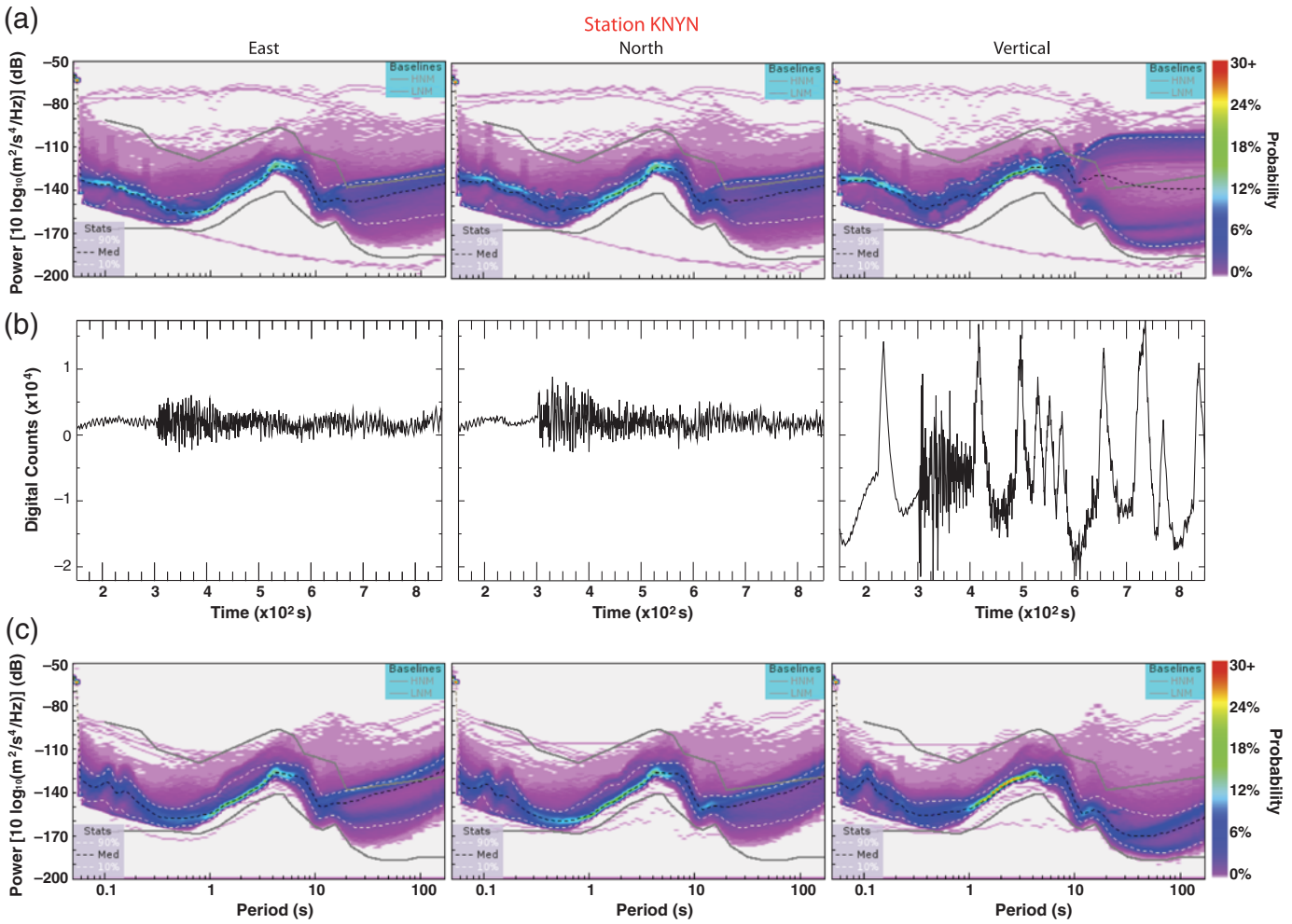

▲ **Figure 6.** (a) SQLX spectral analysis plots for each component of station KNYN during the first year of deployment (18 November 2012 to 17 November 2013). Annotations are the same as for Figure 5a. (b) Example waveform data, showing an 7.0 event that occurred on 6 April 2013 in Irian Jaya, Indonesia. The high-amplitude pinging affecting the vertical component can be clearly seen. (c) Same as (a) but for the second year of deployment (19 November 2013 to 12 November 2014), when the seismometer was changed from a Güralp CMG-3T to a Nanometrics Trillium 240 (T240).

We highlighted the operation and performance of the 15-station TAMNNET array, which was installed in November–December 2012 to provide seismic coverage of the northern TAMs. Data from this network are being used to characterize the crustal and upper-mantle structure beneath the mountain range and to assess competing uplift models. Two years of continuous data have been successfully acquired, and a third year of data will be collected in late 2015. Although some of the stations experienced technical issues, data recovery to date averages ~95%, with most stations displaying high data quality. Using both SOH and waveform data files, along with SQLX spectral analysis, equipment problems in the field have been quickly diagnosed and corrected.

DATA AND RESOURCES

Data from TAMNNET station KNYN are publically available (under network code ZJ) through the Incorporated Research Institutions for Seismology (IRIS) Data Management Center (DMC). Following a 2 yr embargo, all other TAMNNET data will also be available from this source. Metadata is currently available at http://ds.iris.edu/mda/ZJ?timewindow=2012-2016 (last accessed August 2015). Some plots were made using the Generic Mapping Tools software, v.4.5.2 (http://www.soest.hawaii.edu/gmt, last accessed May 2015; Wessel and Smith, 1998).

ACKNOWLEDGMENTS

We would like to thank the Transantarctic Mountains Northern Network (TAMNNET) field team, the Antarctic Support Contractor, the Incorporated Research Institutions for Seismology–Program for the Array Seismic Studies of the Continental Lithosphere (IRIS-PASSCAL) facility, and the National Science Foundation (NSF) for their logistical support. We also thank Editor-in-Chief Zhigang Peng and two anonymous reviewers for their thorough critiques of this article. Data handling assistance has been provided by the IRIS Data Management Center (DMC).

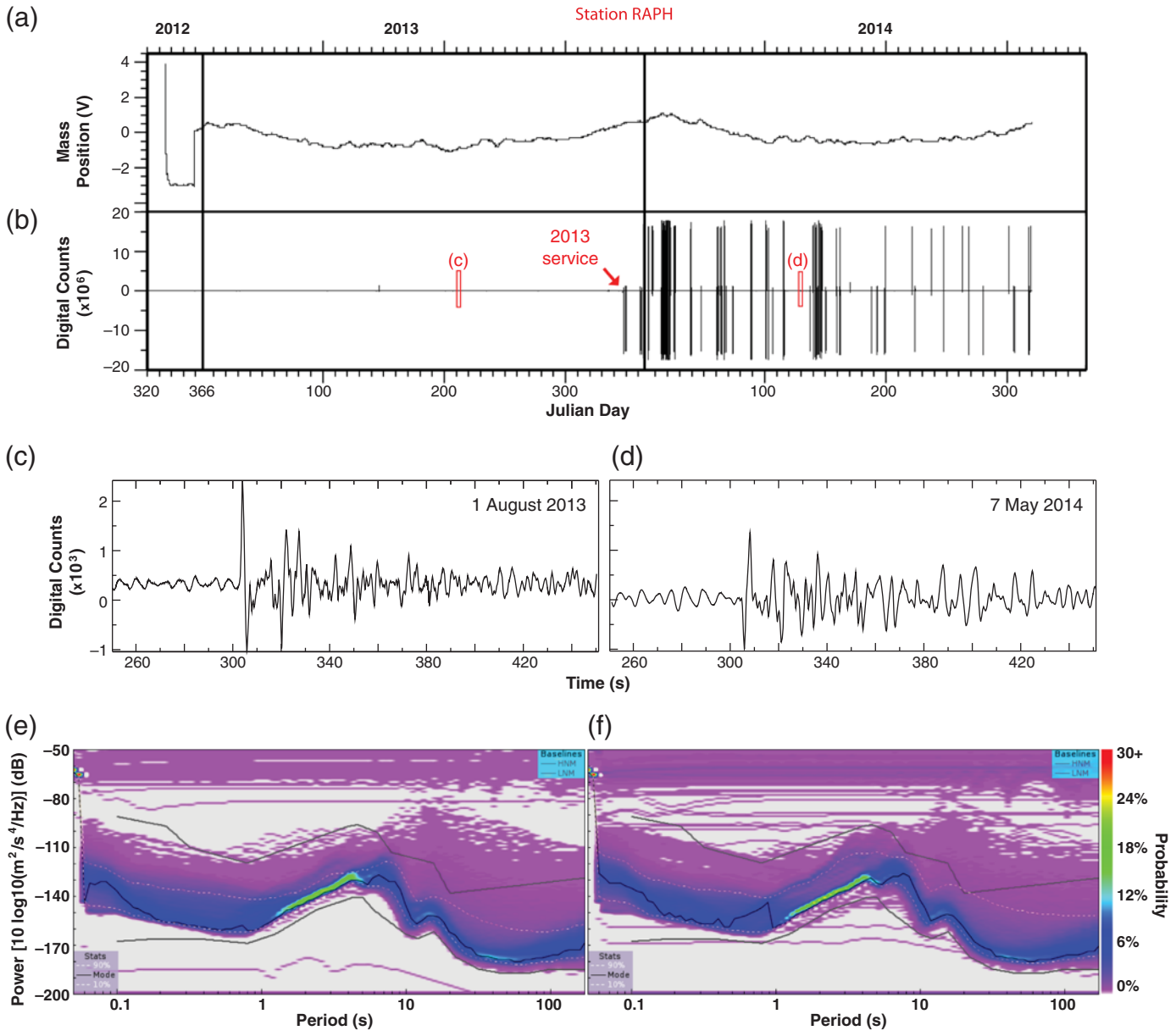

▲ **Figure 7.** (a) Mass position and (b) waveform data for the vertical component of station RAPH as a function of deployment time. Records of two 6.0 earthquakes are denoted by the red boxes on (b) and are highlighted in (c) and (d). The associated SQLX spectral analysis results for the first year (30 November 2012 to 29 December 2013) and second year (29 December 2013 to 16 November 2014) of deployment are shown in (e) and (f), respectively. Annotations for (e) and (f) are the same as for Figure 5a.

The facilities of the IRIS Consortium are supported by the NSF under cooperative agreement EAR-1063471, the NSF Office of Polar Programs, and the Department of Energy National Nuclear Security Administration. Funding for this project was provided by NSF Grant ANT-1139739.

REFERENCES

Anandakrishnan, S., D. E. Voigt, P. G. Burkett, B. Long, and R. Henry (2000). Deployment of a broadband seismic network in West Antarctica, *Geophys. Res. Lett.* **27,** 2053–2056.

Anthony, R. E., R. C. Aster, D. Wiens, A. Nyblade, S. Anandakrishnan, A. Huerta, J. P. Winberry, T. Wilson, and C. Rowe (2015). The seismic noise environment of Antarctica, *Seismol. Res. Lett.* **86,** no. 1, 89–100, doi: 10.1785/0220140109.

Anthony, R. E., R. C. Aster, D. A. Wiens, A. Nyblade, and C. A. Rowe (2011). Seismic noise levels across Antarctica, *AGU Fall Meeting*, San Francisco, California, 5–9 December 2011, Abstract Number 2204.

Bannister, S., J. Yu, B. Leitner, and B. Kennett (2003). Variations in crustal structure across the transition from West to East Antarctica, Southern Victoria Land, *Geophys. J. Int.* **155,** 870–884.

Barrett, P. J. (1981). History of the Ross Sea region during the deposition of the Beacon supergroup 400–180 million years ago, *J. Roy. Soc. New Zeal.* **11,** 447–458.

Barrett, P. J., M. J. Hambrey, D. M. Harwood, A. R. Pyne, and P. N. Webb (1989). Synthesis—Antarctic Cenozoic history from the CIROS-1 drill hole, McMurdo Sound, *DSIR Bull.* **245,** 241–251.

Behrendt, J. C., and A. K. Cooper (1991). Evidence of rapid Cenozoic uplift on the shoulder escarpment of the Cenozoic West Antarctic rift system and a speculation on possible climate forcing, *Geology* **19,** 315–319.
Bialas, R. W. (2009). Models of continental extension and exhumation: Influence of plateau collapse, sedimentation, dike injection, and slab rollback, *Ph.D. Dissertation*, Columbia University, New York.
Bialas, R. W., W. R. Buck, M. Studinger, and P. G. Fitzgerald (2007). Plateau collapse model for the Transantarctic Mountains—West Antarctic Rift System: Insights from numerical experiments, *Geology* **35,** 687–690.
Butler, R., T. Lay, K. Creager, P. Earl, K. Fischer, J. Gaherty, G. Laske, B. Leith, J. Park, M. Ritzwoller, *et al.* (2004). The global seismographic network surpasses its design goal, *Eos Trans. AGU* **85,** 225–229.
Chaput, J., R. C. Aster, A. Huerta, X. Sun, A. Lloyd, D. Wiens, A. Nyblade, S. Anandakrishnan, J. P. Winberry, and T. Wilson (2014). The crustal thickness of West Antarctica, *J. Geophys. Res.* **119,** no. 1, 378–395, doi: 10.1002/2013JB010642.
Clapperton, C. M., and D. E. Sugden (1990). Late Cenozoic glacial history of the Ross embayment, Antarctica, *Quaternary Sci. Rev.* **9,** 253–272.
Fitzgerald, P. G. (1992). The Transantarctic Mountains of southern Victoria Land: The application of apatite fission track analysis to a rift shoulder uplift, *Tectonics* **11,** 634–662.
Fitzgerald, P. G. (1994). Thermochronologic constraints on post-Paleozoic tectonic evolution of the central Transantarctic Mountains, Antarctica, *Tectonics* **13,** 818–836.
Fitzgerald, P. G., M. Sandiford, P. J. Barrett, and A. J. W. Gleadow (1986). Asymmetric extension associated with uplift and subsidence in the Transantarctic Mountains and Ross embayment, *Earth Planet Sci. Lett.* **81,** 67–78.
Fretwell, P., H. D. Pritchard, D. G. Vaughan, J. L. Bamber, N. E. Barrand, R. Bell, C. Bianchi, R. G. Bingham, D. D. Blankenship, G. Casassa, *et al.* (2013). BEDMAP2: Improved ice bed, surface and thickness datasets for Antarctica, *Cryosphere* **7,** 375–393.
Hansen, S. E., J. Julià, A. A. Nyblade, M. L. Pyle, D. A. Wiens, and S. Anandakrishnan (2009). Using *S* wave receiver functions to estimate crustal structure beneath ice sheets: An application to the Transantarctic Mountains and East Antarctic craton, *Geochem. Geophys. Geosys.* **10,** no. 8, doi: 10.1029/2009GC002576.
Heeszel, D. S., D. A. Wiens, A. A. Nyblade, S. E. Hansen, M. Kanao, M. An, and Y. Zhao (2013). Rayleigh wave constraints on the structure and tectonic history of the Gamburtsev Subglacial Mountains, East Antarctica, *J. Geophys. Res.* **118,** 2138–2153.
Huerta, A. D., and D. L. Harry (2007). The transition from diffuse to focused extension: Modeled evolution of the West Antarctic rift system, *Earth Planet. Sci. Lett.* **225,** 133–147.
Johns, B., K. R. Anderson, B. C. Beaudoin, J. Fowler, T. Parker, and S. White (2006). Development of a power and communications system for remote autonomous polar observations, *Eos Trans. AGU* **87** (Fall Meet. Suppl.), Abstract S41A-1314.
Karner, G. D., M. Studinger, and R. E. Bell (2005). Gravity anomalies of sedimentary basins and their mechanical implications: Application to the Ross Sea basins, West Antarctica, *Earth Planet Sci. Lett.* **235,** 577–596.
Lawrence, J. F., D. A. Wiens, A. A. Nyblade, S. Anandakrishnan, P. J. Shore, and D. Voigt (2006a). Rayleigh wave phase velocity analysis of the Ross Sea, Transantarctic Mountains, and East Antarctica from a temporary seismograph array, *J. Geophys. Res.* **111,** no. B6, doi: 10.1029/2005JB003812.
Lawrence, J. F., D. A. Wiens, A. A. Nyblade, S. Anandakrishnan, P. J. Shore, and D. Voigt (2006b). Crust and upper mantle structure of the Transantarctic Mountains and surrounding regions from receiver functions, surface waves, and gravity: Implications for uplift models, *Geochem. Geophys. Geosyst.* **7,** no. 10, doi: 10.1029/2006GC001282.
McNamara, D. E., and R. P. Buland (2004). Ambient noise levels in the continental United States, *Bull. Seismol. Soc. Am.* **94,** 1517–1527.
Nanometrics (2005). *Trillium 120P Seismometer User Guide*, Nanometrics, Inc., Kanata, Ontario.
Nanometrics (2015). *SQLX: Quality Assessment Tool*, Nanometrics, Inc., Kanata, Ontario.
Parker, T., B. Beaudoin, B. Bonnett, J. Fowler, and K. Anderson (2008). Design and implementation of cold-hardened seismic stations, *EGU General Assembly*, Vienna, Austria, 13–18 April 2008, Vol. 10, Geophys. Res. Abstr. EGU2008-A-00191.
Peterson, J. (1993). Observation and modeling of seismic background noise, *U.S. Geol. Surv. Tech. Rept. 93-322*, 1–95.
Pyle, M. L., D. A. Wiens, A. A. Nyblade, and S. Anandakrishnan (2010). Crustal structure of the Transantarctic Mountains near the Ross Sea from ambient seismic noise tomography, *J. Geophys. Res.* **115,** no. B11, doi: 10.1029/2009JB007081.
Reusch, A. M., A. A. Nyblade, M. H. Benoit, D. A. Wiens, S. Anandakrishnan, D. Voigt, and P. J. Shore (2008). Mantle transition zone thickness beneath Ross Island, the Transantarctic Mountains, and East Antarctica, *Geophys. Res. Lett.* **35,** doi: 10.1029/2008GL033873.
Robinson, E., and J. Splettstoesser (1986). Structure of the Transantarctic Mountains determined from geophysical surveys, in *Geology of the Central Transantarctic Mountains*, M. D. Turner and J. F. Splettstoesser (Editors), Antarct. Res. Series 36, American Geophysical Union, Washington, D.C., 119–162, doi: 10.1029/AR036p0119.
Studinger, M., R. E. Bell, W. R. Buck, G. D. Karner, and D. D. Blankenship (2004). Sub-ice geology inland of the Transantarctic Mountains in light of new aerogeophyiscal data, *Earth Planet Sci. Lett.* **220,** 391–408.
Sutherland, R., N. Mortimer, P. Fitzgerald, and M. Isaac (2011). Age of formation of the Transantarctic Mountains in relation to reorganization of adjacent oceanic plate boundaries, *Int. Symp. Ant. Earth Sci.*, Edinburgh, Scotland, 10–16 July 2011, Abstract PS11.11.
ten Brink, U. S., R. I. Hackney, S. Bannister, T. A. Stern, and Y. Makovsky (1997). Uplift of the Transantarctic Mountains and the bedrock beneath the East Antarctic ice sheet, *J. Geophys. Res.* **102,** 27,603–27,621.
van Wijk, J. W., J. F. Lawrence, and N. W. Driscoll (2008). Formation of the Transantarctic Mountains related to extension of the West Antarctic rift system, *Tectonophysics* **458,** 117–126.
Watson, T., A. Nyblade, D. A. Wiens, S. Anandakrishnan, M. Benoit, P. J. Shore, D. Voigt, and J. VanDecar (2006). *P* and *S* velocity structure of the upper mantle beneath the Transantarctic Mountains, East Antarctic craton, and Ross Sea from travel time tomography, *Geochem. Geophys. Geosyst.* **7,** no. 7, doi: 10.1029/2005GC001238.
Wessel, P., and W. Smith (1998). New, improved version of the Generic Mapping Tools released, *Eos Trans. AGU* **79,** 579.

Samantha E. Hansen
Jordan H. Graw
Gregory R. Brenn
The University of Alabama
Department of Geological Sciences
201 7th Avenue
Tuscaloosa, Alabama 35487 U.S.A.
shansen@geo.ua.edu

Angela M. Reusch
Timothy Parker
Douglas K. Bloomquist
Paul Carpenter
Incorporated Research Institutions for Seismology–Program for the Array Seismic Studies of the Continental Lithosphere (IRIS-PASSCAL) Instrument Center
New Mexico Institute of Mining and Technology
100 East Road
Socorro, New Mexico 87801 U.S.A.